On Internal Erosion of the Pervious Foundation of Flood Protection Dikes

Laurence Girolami, Stéphane Bonelli, Rémi Valois, Naïm Chaouch, Jules Burgat

water

MDPI

Brief Report

On Internal Erosion of the Pervious Foundation of Flood Protection Dikes

Laurence Girolami [1,2,*], Stéphane Bonelli [1], Rémi Valois [3], Naïm Chaouch [1] and Jules Burgat [1]

[1] RECOVER, INRAE Aix-Marseille Université, 13182 Aix-en-Provence, France
[2] GéHCO, Campus Grandmont, Université de Tours, 37020 Tours, France
[3] EMMAH, INRAE Université de Avignon, 84914 Avignon, France
* Correspondence: laurence.girolami@inrae.fr

Abstract: This work focuses on the mechanisms that trigger internal erosion of the pervious foundation of flood protection dikes. The origin of these permeable layers is generally attributed to the presence of a paleo-valley and paleo-channels filled with gravelly-sandy sediments beneath the river bed and dikes. These layers may extend into the protected area. Visual observations of leaks, sand boils and sinkholes in the protected area testify to internal erosion processes in the underground soil. Local geological conditions are part of the information to be sought to explain these processes: presence of permeable soils and position of interfaces. Results obtained on Agly dikes (France), using two classical geophysical methods (EMI and ERT), were analyzed using cored soils and showed that it is not enough to simply conclude to the presence of backward erosion piping. The possibility of internal erosion, such as suffusion or contact erosion, must also be considered as the cause of leaks, sand boils and sinkholes. As the results obtained are explained by the presence of a paleo-valley and paleo-channels beneath the river bed and dikes—commonly encountered in this context—the methodology presented and the results obtained are likely to be relevant for many dikes.

Keywords: river dikes; levees; paleo-valley; paleo-channels; leaks; internal erosion; sand boils; sinkholes; geophysical observations; electrical conductivity

Citation: Girolami, L.; Bonelli, S.; Valois, R.; Chaouch, N.; Burgat, J. On Internal Erosion of the Pervious Foundation of Flood Protection Dikes. *Water* **2023**, *15*, 3747. https://doi.org/10.3390/w15213747

Academic Editors: Vlassios Hrissanthou, Mike Spiliotis and Konstantinos Kaffas

Received: 4 September 2023
Revised: 18 October 2023
Accepted: 24 October 2023
Published: 26 October 2023

1. Introduction

Protection dikes help keeping safe urban populations settled along rivers from risks encountered by flooding events. Underlying soils, termed as foundation, are however prone to internal erosion, which represents one of the main causes of breach failures [1,2]. This process results from the transport and migration of soil particles subjected to localized flows. Internal erosion processes include erosion along a crack or a pre-formed hole (concentrated leak erosion), migration of the fine fraction through a coarse matrix (suffusion), erosion along a contact between two soils (contact erosion), and erosion starting from a point of loss of effective stress by fluidization [3] and propagating backward towards upstream (backward erosion piping) [4–6]. Observations of surface signatures (leaks, sand boils, sinkholes and turbidity) represent the most relevant evidences of internal erosion.

The most documented signatures, termed as *sand boils*, are recognized as one of the major causes of severe damage or even failure of flood defenses worldwide [7–9]. Different mechanisms have been identified as being responsible of them [10]: detour and reappearance of a sediment-laden subsurface flow along a pre-existing fissure; earthquake-induced liquefaction; landslides; and subsurface flow under artesian conditions. The last case, discussed in this study, is driven by the imbalance of hydraulic head on both sides of the dike: the river and the protected area. As the water level rises during floods, a significant hydrostatic imbalance is formed across the foundation, increasing the pore pressure gradient and thus decreasing the effective stress acting on soil particles, which promotes their erodibility through seepage flows. Above a threshold velocity, the flow becomes strong enough to detach sand particles from the underlying soil located beneath

the protected area and transport them across the cover layer of variable thickness. At this point, the hydraulic gradient quickly dissipates, depositing eroded material around the pipe head. The deposit, termed as sand boil, has a conical shape and is mostly made with fine sand. Once triggered, erosion can gradually progress towards the riverside, creating shallow pipes within the sand layer that can impede the dike stability.

Sand boils can also indicate local heave initiated at much lower hydraulic head than required for pipe progression, meaning that the process may stop at a constant hydraulic head [11]. In this case, the presence of sand boils may not lead to breach failures but can promote a late piping initiation during future periods of equivalent water levels, assuming that the duration of erosion processes is much longer than that of a flood and that pipes remain intact after flooding events. The description of such processes has become the priority of dike managers in charge of the safety of the embankment system.

Current analyses only integrate fine-scale information relating to soil and layer geometry, within a simplified description [11–14]. A broad majority of studies consider that the sand layer is horizontal within the foundation, and that such processes typically start along natural weaknesses or holes in the ground where flows are concentrated. However, such analyses cannot explain the position of sand boils around levee toes, or in their vicinity, up to 1 km [15]. While such specific hydraulic phenomena are presently well understood, the appearance of sand boils and their location relative to the dike remains difficult to predict. Local geological conditions are rarely considered, even though they have a major influence on sand boil distribution [16–18]. These local geological conditions may however explain why many kilometers of levees experience similar hydraulic gradients, but different symptoms at the surface: no signature, leaks or sand boils, and justify why few present physical and numerical models are capable of reproducing such observations made around protection dikes [19].

Another important erosion signature, widely observed around protection dikes, and described in the literature is defined as *sinkholes*. Different types of sinkholes have been reported, depending on the rocky, karstic, or granular nature of the environment [20]. The appearance of sinkholes in soils is a phenomenon that most often results from the collapse of a very low-density, mechanically unstable volume of soil. When this volume of soil is located in depth, the entire column of soil above settles. Low local density may be the result of internal erosion: suffusion [21,22] or contact erosion [23]. Settlement due to mechanical instability can occur immediately during significant erosion (when the soil is saturated), or later, when the previously eroded soil is dry and subject to saturation. Although sinkholes are observed on dikes in a non-karstic setting [7,8,24,25], the origin of these phenomena is still difficult to explain [26] and their modeling is complex [27]. Up to now, no studies have been proposed to explain their formation in foundation soils of river dikes that consider local geological conditions.

Although the observation of leaks, sand boils and sinkholes is commonly incorporated into risk analyses through expert judgement, local geological conditions are rarely considered. This work therefore aims at proposing geological observation of the foundation soils located beneath and around dikes locally affected by internal erosion, using both ElectroMagnetic Induction (EMI) and Electric Tomography (ERT) methods commonly used for river levees [28,29]. This study provides new information on the subsurface soils located beneath dikes and protected areas (nature of soils and position of interfaces), making it possible to formulate new hypotheses concerning the causes of leaks, sand boils and sinkholes. The importance of knowing local geological conditions is illustrated by the case of Agly dikes, where numerous leaks, sand boils and sinkholes have been frequently observed after floods (Figure 1), but have not yet been described [7,8,30]. Results obtained are explained by the presence of a paleo-valley and paleo-channels beneath the river bed and dikes, which are commonly encountered in this context. By using the methodology presented, the results obtained are likely to apply to numerous dikes.

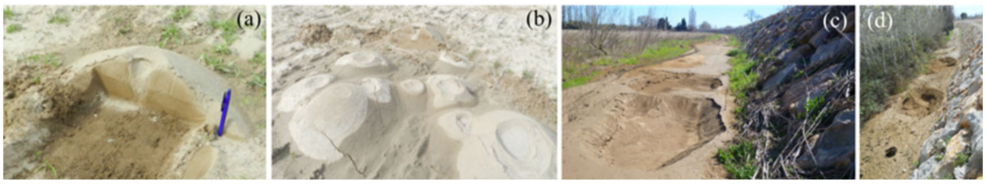

Figure 1. (**a**,**b**) Sand boils in the protected area, (**c**,**d**) Sinkholes observed around the levee toe.

2. Sand Boils and Sinkholes along the Agly Dikes

Geomorphological analyses have revealed that the Agly River is a perched river, whose minor bed is located above the natural ground of the area protected by dikes. The studied area is located downstream of a sharp widening of the major bed, leaving the possibility for the river to expand [31]. The geological context is characterized by recent Quaternary alluvial deposits of the river that may imply the probable presence of a paleo-valley and paleo-channels in the foundation soil, with a possible complex geometry. This information helps us to understand the presence of lenses of high-graded soil beneath the levees and their non-regular layouts.

Between 1969 and 1974, 13 km of dikes of 2–3 m high above the floodplain with a crest of 8 m wide, were built along the river bed of approximately 65 m wide to protect 30,000 people from risks incurred by flooding events. On the river side, the height is assessed as around 6 m, while a berm is located at mid-height of the protected area. The levee core consists of sandy loam to silty sand, while a 2 m deep drainage spur, topped with riprap, was built downstream after the flooding episode of 6 March 2013.

The diking system has been exposed to 11 floods over the period 1977–2020. Floods usually last for a few hours. The event of 1999 caused a breach on the northern bank, resulting in 35 victims, with a peak discharge of around 2110 m^3/s. Later, the 2013 flooding event caused a breach on the southern bank, with a peak flow of around 970 m^3/s. Geotechnical investigations highlighted the heterogeneous nature of the substratum and led to its simplified description: a superficial sandy silts to silty sands layer of highly variable thickness (from a few cm to 5 m), covering a roughly flat sandy layer (from fine to coarse) of up to 10 m deep above the impermeable basement, also containing highly permeable coarse materials (gravels, boulders, pebbles, cobbles), resulting from the river recalibration, and described in the borehole logs carried out after the 2013 flooding event (Figure 2b).

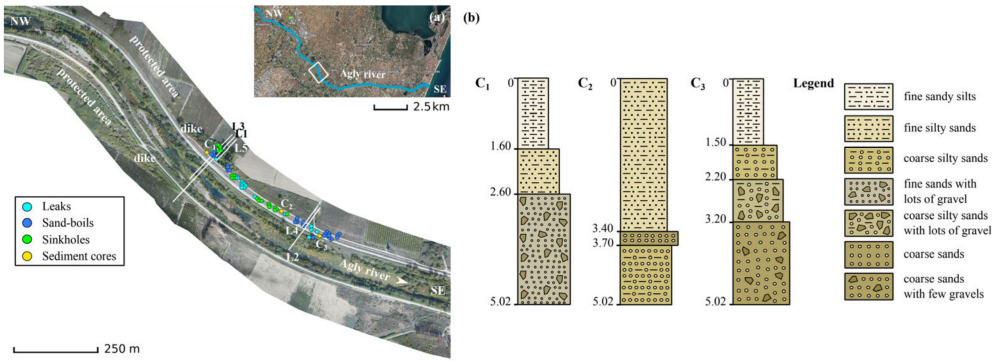

Figure 2. (**a**) Study area where both location of leaks, sand boils and sinkholes on the northern bank, as well as transverse ERT lines, have been reported. (**b**) Examples of borehole logs (C_1, C_2, C_3) performed in the area of interest and located on the map, that highlight the presence of coarse-grained soils constituting the permeable layers over a thickness of up to 5 m deep.

After each of the six floods reported from 1992 to 2014, leaks, sand boils and sinkholes were observed around dikes (Figure 1). Sand boils formed very regular cones of up to 1 m in diameter and were observed along two sections: a 700 m long section located down the northern bank; and a 500 m long section located down the southern bank, at up to around 60 m from the levee toe (Figures 1 and 2a). Additionally, sinkholes often assimilated

to collapsed sand boils, were observed close to the levee toe, and exposed an irregular ellipsoidal shape of around 0.5 to 3 m long with an almost flat basement (Figure 1).

A granulometric analysis of sand boils observed in 1999, 2006 and 2013 showed that the cones were made with sandy materials, while the surrounding subsoil was composed of very little clay (a few %), sand (from 30 to 90%), and silt (from 10 to 40%) [7,8,30]. Three examples of borehole logs in the subsurface soil are given in Figure 2b.

To date, no satisfactory explanation exists to describe the appearance of leaks, sand boils and sinkholes around dikes, nor any modeling is able to reproduce these observations [7,8,30].

3. Materials and Methods

3.1. Description of Geophysical Methods

The aim of these observations is to highlight the importance of geological conditions in providing information required to explain the presence of leaks, sand boils and sinkholes. On the site studied, such information was obtained using two classical geophysical methods [28]: Electromagnetic Induction Method (EMI) and Electric Resistivity Tomography (ERT).

EMI is a well-established option for mapping the subsurface soil in a horizontally continuous manner. This method is well suited to acquire measurements of apparent electrical conductivity (in S/m; where 1 Siemens = 1 Ohm^{-1}) of the subsurface soil. The procedure consists in using coils in which an alternating current is flowing with a known frequency. Such measurements, performed by wearing the device and walking along parallel lines, provides a quick and cost-effective investigation along foundation dikes.

ERT can furthermore capture vertical information by acquiring measurements of apparent electrical resistivity (Ω.m) by injecting a current of known intensity in soils through a pair of electrodes, while measuring the potential drop which depends on the material properties through another pair of electrodes. Apparent values can thus be transformed into local real electrical resistivity after inversion processes that capture two-dimensional (2D) vertical sections of soils. The depth of investigation and resolution both depend on electrode spacing, device length, acquisition network and the investigated natural material. Resolution decreases with increasing depth of investigation.

3.2. Testing Protocols Followed on the Field

EMI was performed with a Geonics EM31-MK2. The apparent electrical conductivity of the soil was averaged over the first 6 m deep. Acquisition was carried out by walking at a velocity of around 1 m/s. A GPS was coupled to measurements. The acquisition period was taken of one second, leading to a spacing of around 1 m between each measurement. The paths were not always straight because of the vegetation, whereas the field remained approximately flat.

Three profiles were positioned owing to the repeated observations of leaks, sand boils and sinkholes made after the 2013 flooding event. One transverse profile, performed at the scale of the diked bed (L1), was made possible because of the river drought; two additional profiles were made at the scale of the levee (L2 and L3) while two more accurate profiles were made at the scale of the erosion symptom (leaks and sand boils L4; sinkholes L5). All profiles, presented here, were orthogonal to the levee (Figure 2), and assumed parallel to the underlying seepages. The characteristics of the profiles are given in Table 1. The profiles involved 64 to 120 electrodes. The inversion of apparent resistivity data was carried out using ResiPy [32].

Table 1. Characteristics of the geophysical profiles.

ERT Profiles	Equipment	Electrodes Spacing–Length	Array Type	Measurements Nb per Profile	Period of Measurements
L1	IRIS Syscal Pro	2–238 m	Wenner–Schlumberger	3254	Spring 2023
L2, L3	ABEM SAS4000	2–126 m	Wenner-α	472	Spring 2023
L4, L5	ABEM LS 2	1–63 m	Wenner-α	472	Spring 2022

4. EMI and ERT Results

To a first approximation, the lowest electrical conductivity values correspond to permeable layers containing silts, sands and gravels, while the highest values correspond to weakly permeable layers containing fine silty and clayey materials.

4.1. EMI Results

EMI measurements reveal two main conductivity zones (Figure 3):

- a zone of values of conductivity inferior to 0.01 S/m, indicating a permeable soil layer mostly made with coarse sands, silts and gravels (Figure 2b);
- a zone of values of conductivity greater than 0.02 S/m, indicating a less-permeable soil layer mostly made with fine silts [7,8,30].

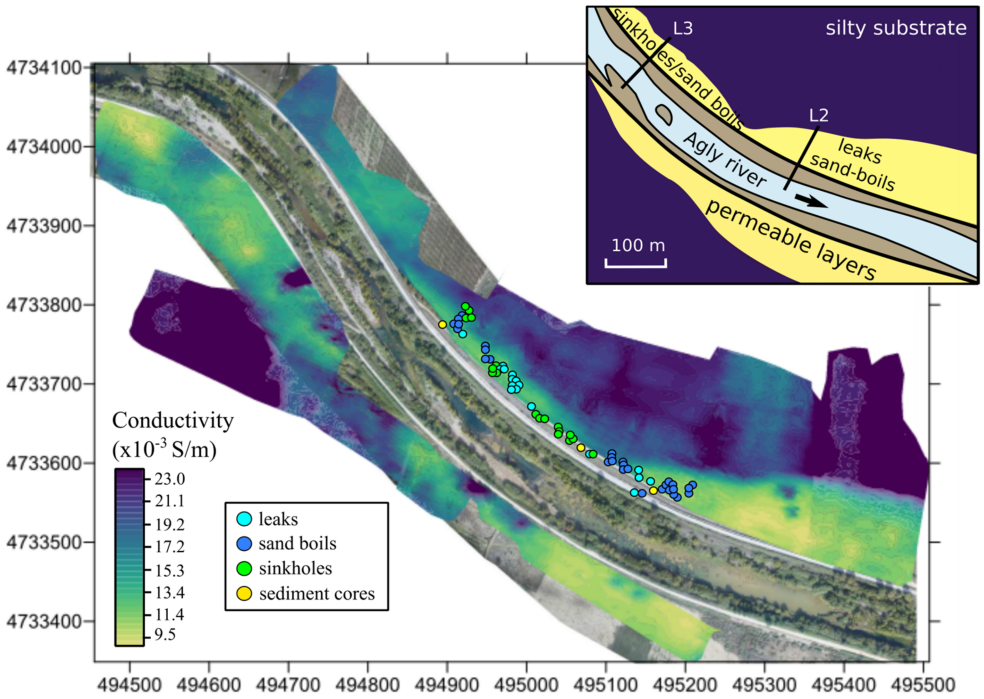

Figure 3. EMI results, map of soil conductivity averaged over the first 6 m deep. The scheme highlights two main areas where erosion signatures have been observed.

4.2. ERT Results

Values scales used in Figures 4–6 are identical to those used in Figure 3, while both conductivity and resistivity are given, so that EMI and ERT results can be compared. Figure 4 reveals two main conductivity regions:

- an area of conductivity measurements below 5×10^{-4} S/m located on the minor bed and beneath the northern and southern embankments, indicating a permeable soil layer that corresponds to old sediments that fill a paleo-valley,

- an area with measurements of conductivity above 7×10^{-3} S/m located in depth, indicating a less-permeable soil layer that corresponds to a sandy-marly substrate, which includes the groundwater at the time of measurements.

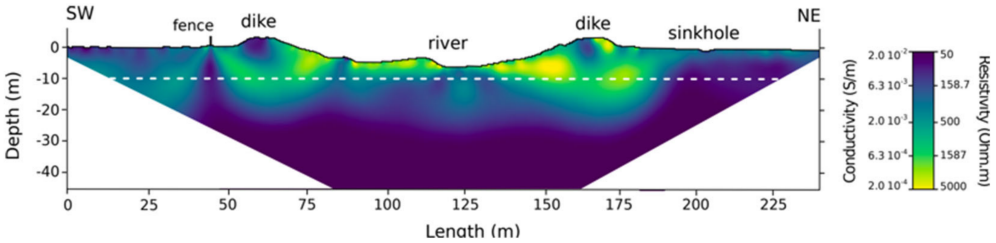

Figure 4. ERT profile along L1, exposing the soil conductivity and resistivity. The white dashed line represents the position of the groundwater. The minor bed was dried up at the time of measurement.

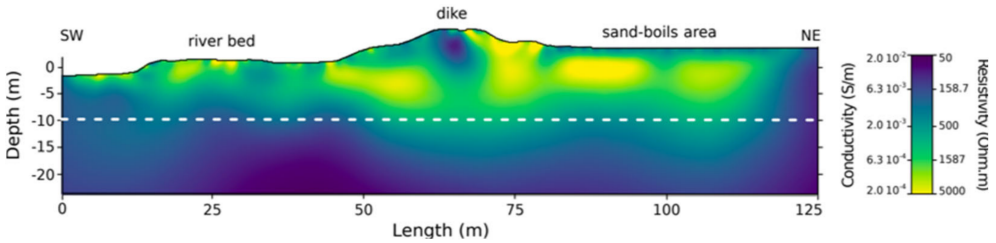

Figure 5. ERT profile along L2, exposing the soil conductivity and resistivity. The white dashed line represents the position of the groundwater. The minor bed was dried up at the time of measurement.

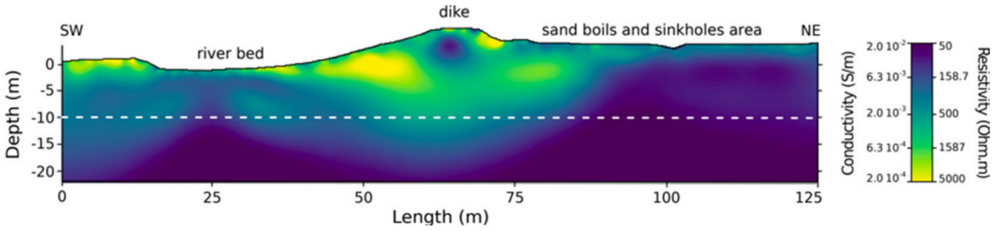

Figure 6. ERT profile along L3, exposing the soil conductivity and resistivity. The white dashed line represents the position of the groundwater. The minor bed was dried up at the time of measurement.

This result shows that paleo-sediments become saturated during a flood and form underlying seepage flows from the diked bed to the protected area. These flows travel under the dikes and circulate into the underlying soil of the protected plain. This is confirmed by profiles L2 (Figure 5) and L3 (Figure 6), which extend beyond around 60 m on each side. However, the geometry of the permeable layer in the subsoil evolves from upstream to downstream, as shown by profiles L4 and L5 (Figures 7 and 8, respectively) that cover the 60 m long area from the dike toe to the protected plain.

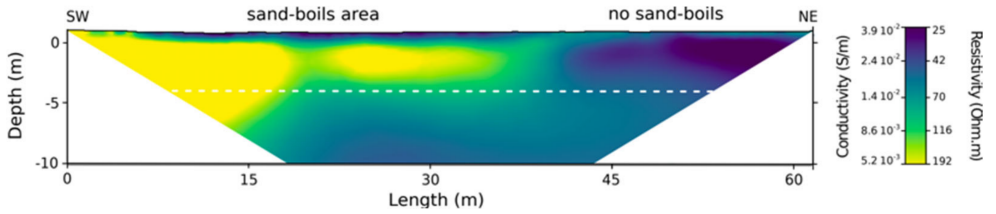

Figure 7. ERT profile along L4, exposing the soil conductivity and resistivity. The white dashed line represents the position of the groundwater. The river was flowing in its minor bed at the time of measurement.

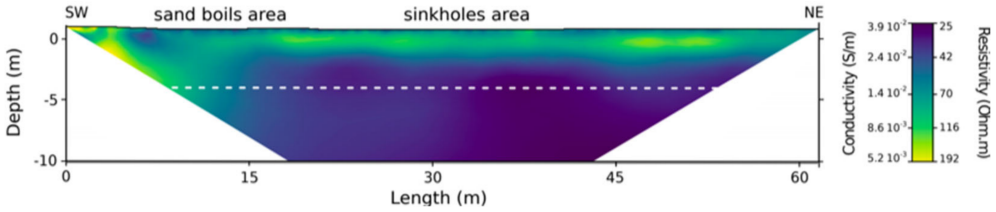

Figure 8. ERT profile along L5, exposing the soil conductivity and resistivity. The white dashed line represents the position of the groundwater. The river was flowing in its minor bed at the time of measurement.

On the site investigated, the followed methodology can be summarized as follows: (i) lateral mapping of averaged soil conductivity (based on EMI) in the protected plains. This mapping showed the presence of permeable soils and identifies vertical interfaces between high permeability and low-permeability soils. (ii) Local cross-section mapping (based on ERT). This mapping confirmed the presence of permeable soils and positions of interfaces. It was carried out at different scales to confirm the results, bearing in mind that ERT alone only provides electrical resistivity gradients, not material interfaces. The key point here was that the relationship between electrical resistivity and permeability was deduced from the analysis of cored soils.

5. Results Analysis

5.1. Analysis of EMI Results

The purpose of averaged conductivity measurements provided by EMI is to laterally delimit layers of different composition, each being roughly homogeneous over the first 6 m deep, in order to have an overview of the situation. In the study area, two different geological structures can be distinguished in the flood plain (Figure 3):

- a sandy, permeable layer (paleo-sediments) that expand from the levee toe, to up to a few tens of meters on the protected area where leaks and sand boils are observed after each flooding event.
- a sandy, permeable layer (paleo-sediments) extending from the levee toe to up to around 20 m on the plain where leaks, sand boils and sinkholes were observed after the 2013 flooding event.

5.2. Analysis of ERT Results on Leaks and Sand Boils Locations

The analysis of ERT measurements, shown in Figure 9a, exposes the geometry of this sandy permeable layer, termed a paleo-valley, filled with sediments beneath the levee. This layer is around 15–20 m thick and extends for around 60 m on both sides into the protected plain. Beyond this limit is a less-permeable silty layer, corresponding to the upwelling of a deeper material that reaches the surface, and which may constitute an impermeable barrier preventing the progression of internal flows during flooding events.

Underlying seepage flows have thus two possibilities (Figure 9a): flowing laterally, parallel to the dikes, towards the river mouth (located at around 8 km in a south-east direction), and ascending towards the surface. In any case, the flow can no longer continue in the direction transverse to the levee, since the interface between the permeable and impermeable layer is approximately vertical and extends to the surface. Near the surface, the presence of a thin layer of silty soil, less permeable, promotes the initiation of a heterogeneous fluidization through the formation of more permeable chimneys. This situation corresponds to the conditions of appearance of leaks and sand boils, which can only occur within a thick permeable layer covered by a thin heterogeneous and less permeable one, that widens towards the south-east (Figure 3b).

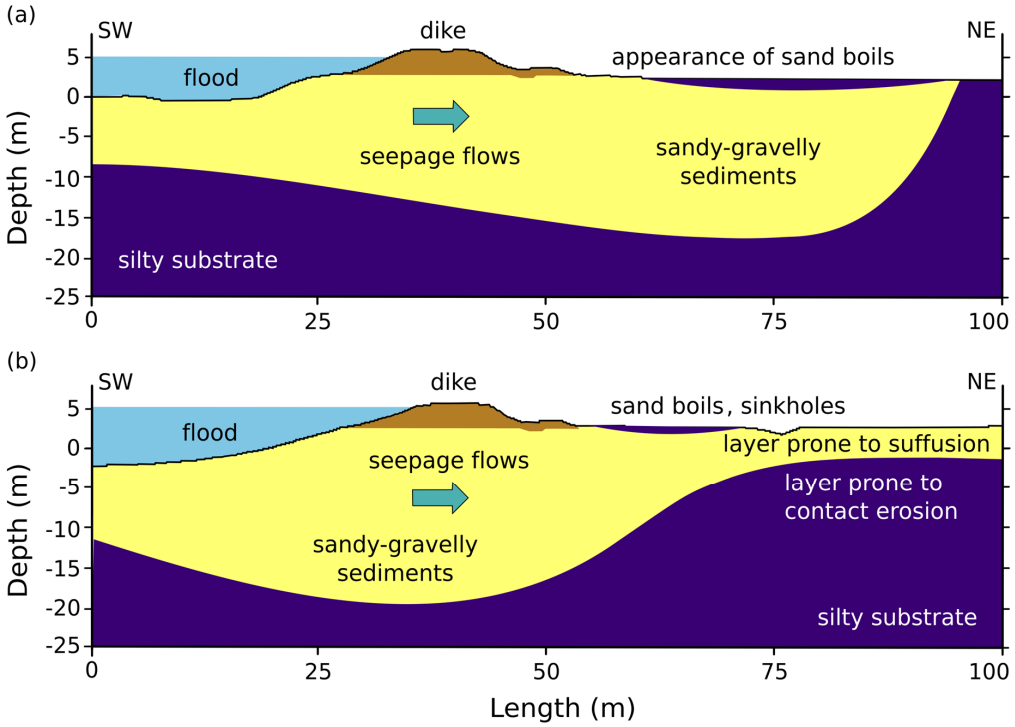

Figure 9. (**a**) ERT results analysis (L2,L4) highlighting the triggering mechanism and possible area of occurrence of leaks and sand boils. (**b**) ERT results analysis along L3, L5 highlighting the three triggering mechanisms and possible area of occurrence of leaks, sand boils and sinkholes above the thinner paleo-channel.

5.3. Analysis of ERT Results on Leaks, Sand Boils and Sinkholes Locations

Interpretation of ERT measurements in Figure 9b shows the geometry of the permeable layer beneath the levee. Its thickness decreases progressively with distance from the levee (from around 10 m to 2 m thick), then becoming approximately constant (when forming a paleo-channel). Beneath this permeable layer lies a less permeable substrate. This means that the internal flow passing beneath the levee can progress into the protected area, over 2 m deep (i.e., five times thinner) and up to 60 m long.

In this area, underlying seepage flows have three possibilities: flowing laterally, parallel to the levee; ascending towards the surface; or progressing in the protected plain until reaching the impermeable limit at a higher velocity due to the reduced thickness of the permeable layer.

Note that underlying seepage flows, parallel to the embankment, may be of less importance when the geometry of interfaces is locally assumed to be parallel to the dike. Otherwise, ascending flows are necessary to explain the appearance of leaks and sand boils at the surface during floods and may be promoted by the presence of an impermeable obstacle formed by the upwelling silty substrate that stops its lateral progression. A thinner surface soil layer, as well as a local hydraulic gradient greater than the initial one, also represent triggering factors for leaks and sand boils formation. Lateral flows, propagating towards the protected area and perpendicular to the levee, are likely to have high local velocity capable of inducing two other types of erosion (Figure 9b): (i) a selective internal erosion (suffusion) in the permeable layer that will locally increase the volume of the pore domain and give the material a possible mechanical instability. The local decompaction of the permeable layer may cause the collapse of its upper limit, as well as the above soil layer and the formation of a sinkhole at the surface. (ii) Contact erosion of the less permeable material, at the interface with the permeable material in depth. The eroded fine soil is transported by the flow into the permeable layer, which locally induces cavities, that if

located superficially (i.e., about 2 m deep), can promote the soil layer collapse and the formation of sinkholes at the surface.

6. Discussion

6.1. Remarks on the Influence of Temperature and Water Content on Resistivity Variations

Although ERT and EMI measurements have been made within two different years, inherent time lapses were not limiting for a relative comparison of the geophysical properties between the different techniques and profiles. As the topography of the study area remains flat, most of the variations of the geophysical properties over time are related to seasonal variations (i.e., temperature and water content). Moreover, to correctly interpret values of electrical resistivity, in terms of soil types, it is important to know the factors influencing resistivity. For a given soil, electrical resistivity decreases with temperature, water content and density. The soils were investigated during spring, with a groundwater located from 5 to 9 m deep. Being highly permeable, the constituting material can be considered as dry, so that variations in resistivity are not attributable to water content for depths up to 5 m. The ambient temperature during measurements ranged from 20 °C to 30 °C. The temperature below 10 m can be estimated to be around 10 °C. The order of magnitude of the influence of the temperature gradient in the soil is therefore 50% on variations in resistivity measurements.

For a given soil, subjected to identical conditions of temperature and water content, values of electrical resistivity may decrease with density. ERT measurements are not well suited to investigate such density gradients as well as to detect the presence of voids; this may require a combination of Ground-Penetrating Radar (GPR) and seismic methods that will be the topic of future research. Additionally, repeating the same ERT profiles for different hydrogeological conditions can improve the knowledge of the soil layers and the location of groundwater bodies during floods or discharge events [33].

Under constant temperature and hydrogeological conditions, electrical resistivity decreases with the volume percent of clays. Analyses of sediment cores and drillings, made on the foundation soils of Agly dikes, expose a composition depleted in clays (less than few %) [7,8,30], which justifies the use of both EMI and ERT here, along with sediment sampling, to map the presence of paleo-valleys and paleo-channels and correlate them to erosion symptoms observed on protected areas.

Observations of leaks, sand boils and sinkholes also involve a combination of several physical processes in the subsurface soil, as well as a complex geometry of permeable and less permeable soil layers. Such processes probably do not consist of only one type of internal erosion, but rather several interacting mechanisms, such as suffusion and contact erosion. Erosion phenomena are described by threshold laws, which requires numerical modeling involving input data that accurately describe the investigated situation, and in particular, the geometry of soil layers and interfaces.

6.2. Numerical Modeling: Example of Results and Comments on Hydraulic Modeling Based on ERT Measurements

Two-dimensional numerical modeling using finite elements was carried out on simplified geometries deduced from the analysis of geophysical results and available soil cores. The mesh comprises 7357 linear elements. Dimensions, boundary conditions and permeabilities are given in Figure 10. The dike is assumed to be of 2 m high, while the water level is at crest on the river side and is taken to be 5 m below the natural ground on the protected area. The surface layer of sandy silt is e = 1 m thick. The two cases shown in Figure 9 were modeled. Figure 10 plots the flow vectors $\boldsymbol{q}$, and the pressure $p(x)$ beneath the surface layer of sandy silt. In both cases, $p(x)$ is very high and can exceed 1.5 m, which turns out to be a favorable condition for the appearance of a resurgence likely to cause erosion. However, in case (a) (Figure 10b), the curve $p(x)$ quickly tends towards zero after the vertical interface, pointing that erosion signatures can appear only between the dike and the vertical interface. In case (b), the values of $p(x)$ remain significant after the vertical interface, showing that

erosion signatures can appear over a wider area, extending beyond the vertical interface. The flow intensity in the gravelly sand layer in the case (b) (Figure 10c) is of one order of magnitude greater than in case (a) (Figure 10b). However, in both cases, flow velocities can be locally of the same order of magnitude as those required for the initiation of suffusion (10^{-6} to 10^{-5} m/s, [34]) in this layer. Carrying out modeling to integrate the different types of erosion requires a finer description, which is beyond the scope of this paper.

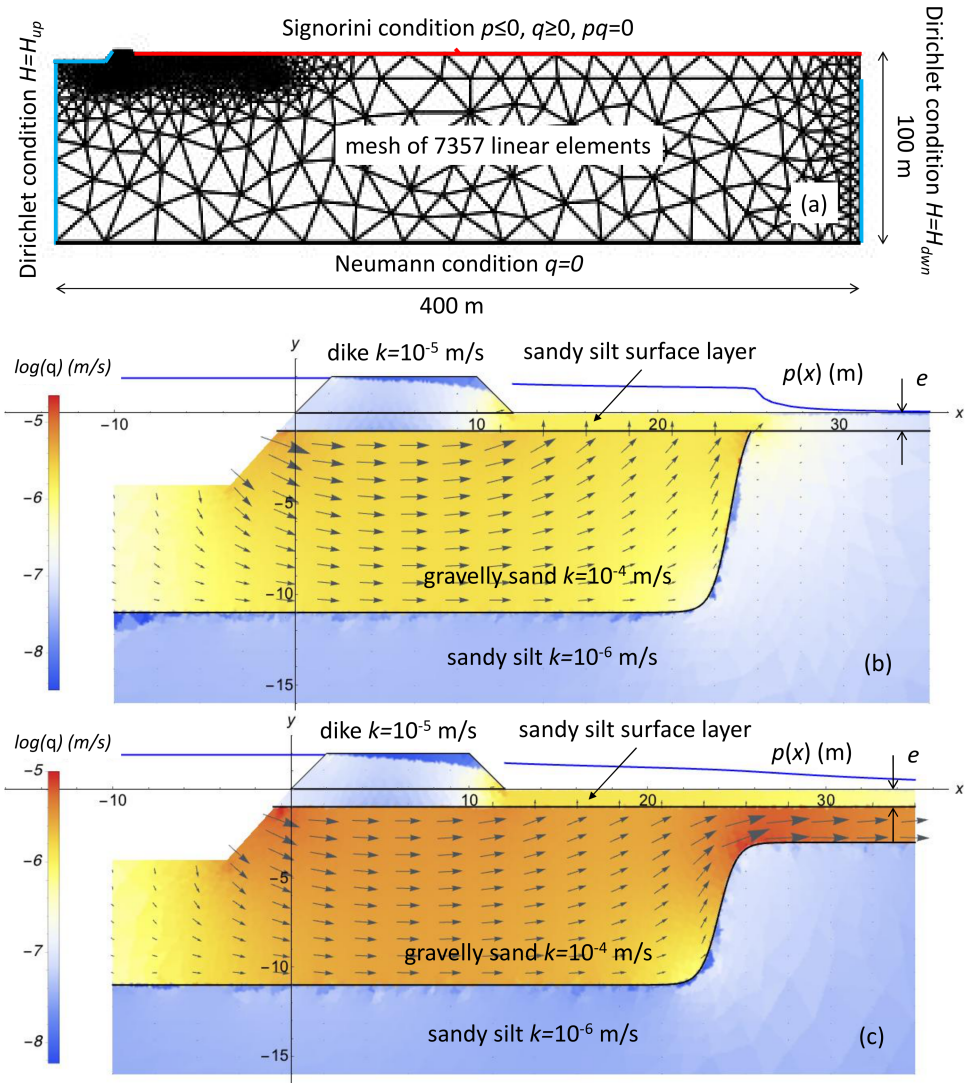

Figure 10. Finite elements modeling implying a simplified geometry. (**a**) Mesh and boundary conditions. (**b**,**c**) Results of the numerical model: flow vectors $\boldsymbol{q}$, isocolor of $\log||\boldsymbol{q}||$, and pressure $p(x) = H(x) - e$ (m) beneath the sandy silt surface layer, of thickness e, for geometries observed and reported on Figure 9a (**b**) and Figure 9b (**c**), where H is the hydraulic head, and k is the permeability.

Specific work is necessary to quantify the permeability of the soils in place, in coherence with the electrical resistivity tomograms, and allow Finite Element Modeling (FEM) of internal flows. In this context, in situ sampling by core drilling in the areas of interest is necessary in order to carry out identification and laboratory tests (particle size analysis and permeability tests). In this example, three-dimensional FEM modeling is necessary to account for the possibility of horizontal flows parallel to the levee.

The permeable zones here are correlated with the presence of a paleo-valley filled with sandy-gravelly sediments. The latter must be detected as a priority, by analyzing the geomorphological history of the river and the dike system. The combined use of EMI and ERT methods also represents a rapid and cost-effective solution to continuously map the

subsurface and effectively capture shallow lateral information [22,34]. The key outcome here is a correct description of the geometric variability of the soil layers under the dike and in the protected area. Geophysical imagery is often affected by a lack of resolution, and the geometry of interfaces is directly estimated by these methods, which inherently lack accuracy. In addition to EMI and ERT, results of geotechnical investigations, e.g., Cone Penetration Test (CPT), core sampling and borehole drilling logs, should be used to directly identify interfaces between soil layers [35].

An accurate description of the layers geometry and their interfaces is crucial to assess the reliability of the diking system, by quantifying the occurrence of the different erosion processes and their kinetics. In the case of the Agly River dikes, flood duration (lasting up to a few hours) may involve high erosion kinetics, which implies high local flow velocities. These latter require more elaborated modeling than a simple approach assuming a simplified geometry and an evaluation of the averaged hydraulic gradients, as it is often the case.

7. Conclusions

Visual observations of leaks, sand boils and sinkholes in the protected area provide evidence of internal erosion processes in the underground soil. Local geological conditions are part of the information to be sought to explain these processes: presence of permeable soils and position of interfaces. This information was obtained for the studied area by combining two classical geophysical methods (EMI and ERT). Results were interpreted using the analysis of cored soils, in order to correlate the electrical resistivity values to the nature of soils (including the orders of magnitude of permeabilities), and the position of interfaces.

Observations highlight the presence of a gravelly sand layer beneath the river bed and dikes, approximately 300 m wide and 25 m deep, which is comparable to the deposits that filled a paleo-valley resulting from the geomorphological history of the river. Important characteristics were observed: the presence of a surface layer of low permeability made with sandy silt (from 0.5 to 1 m thick), the extension of the gravelly sandy layer (of around 12 to 25 m thick) towards the protected zone, which defines a vertical interface, located at a variable distance from dikes, that preferentially guides the flows towards the surface and provide elements to explain the spatial distribution of erosion signatures during floods.

Given the nature of soils and the heterogeneity of flows, simple occurrence analyses of backward erosion piping are not sufficient to describe these erosion signatures. The possibility of internal erosion, such as suffusion or contact erosion, must also be considered. It is also necessary to consider the granulometry of the materials, and to model the initiation and evolution of erosion processes through further research.

The findings of this work highlight the importance of geological conditions to explain the formation of leaks, sand boils and sinkholes. The presence of a paleo-valley, filled with gravelly-sandy sediments beneath the river bed and dikes, turns out to be frequently encountered, suggesting that the methodology and results presented here are likely to apply to many dikes. EMI and ERT methods appear relevant for the site studied. Possible additional methods can be considered for the area of interest. Imaging results are often affected by a lack of resolution, which means that interfaces cannot be accurately located. Two conditions are necessary for success: a strong contrast between weakly and highly permeable areas, and a direct analysis from geotechnical investigations (Cone Penetration Test CPT, core sampling and borehole drilling logs).

Author Contributions: Both conception of the research work, measurements, analysis, interpretations and writing the manuscript have been made in close collaboration between all the authors. All authors have read and agreed to the published version of the manuscript.

Funding: This research was supported by INRAE (grant from Scientific bet of INRAE, Water department), Region Centre-Val de Loire (contribution of Academic Initiative Project RHEFLEXES/201900134935), and grant from Directorate General for Risk Prevention (DGPR).

Data Availability Statement: Not applicable.

Acknowledgments: We thank the managers of the Agly River dikes (SMBVA, F. Nicoleau) for having provided authorization for this work and for fruitful discussions. We thank the company Naga Geophysics for L4-L5 profiles, as part of a service order on behalf of INRAE; as well as the company Sub-C Marine for the DTM aerial lidar, as part of a service order on be-half of INRAE. We thank Laurent Peyras for his precious advices concerning the preparation of the manuscript.

Conflicts of Interest: The authors declare that they have no known competing financial interests or personal relationships that could have appeared to influence the work reported in this paper.

References

1. Foster, M.; Fell, R.; Spannagle, M. The statistics of embankment dam failures and accidents. *Can. Geotech. J.* **2000**, *37*, 1000–1024. [CrossRef]
2. Danka, J.; Zhang, L.M. Dike failure mechanisms and breaching parameters. *J. Geotech. Geoenviron. Eng.* **2015**, *141*, 04015039. [CrossRef]
3. Amin, A.; Girolami, L.; Risso, F. On the fluidization/sedimentation velocity of a homogeneous suspension in a low-inertia fluid. *Powder Technol.* **2021**, *391*, 1–10. [CrossRef]
4. Fell, R.; Fry, J.-J. (Eds.) *Internal Erosion of Dams and Their Foundations*; Taylor & Francis: London, UK, 2007.
5. Bonelli, S. (Ed.) *Erosion of Geomaterials*; John Wiley & Sons: Hoboken, NJ, USA, 2012; 371p.
6. Bonelli, S. (Ed.) *Erosion in Geomechanics Applied to Dams and Levees*; John Wiley & Sons: Hoboken, NJ, USA, 2013; 388p.
7. Zwanenburg, C.; López-Acosta, N.P.; Tourment, R.; Tarantino, A.; Pozzato, A.; Pinto, A. Lessons Learned from Dike Failures in Recent Decades. *Int. J. Geoengin. Case Hist.* **2017**, *4*, 203–229.
8. Van, M.A.; Rosenbrand, E.; Tourment, R.; Smith, P.; Zwanenburg, C. Failure paths for levees. International Society of Soil mechanics and Geotechnical Engineering (ISSMGE)—Technical Committee TC201 'Geotechnical aspects of dikes and levees'. 2022.
9. Richards, K.S.; Reddy, K.R. Critical appraisal of piping phenomena in earth dams. *Bull. Eng. Geol. Environ.* **2007**, *66*, 381–402. [CrossRef]
10. Holzer, T.L.; Clark, M.M. Sand boils without earthquakes. *Geology* **1993**, *21*, 873–876. [CrossRef]
11. van Beek, V.M. Backward Erosion Piping: Initiation and Progression. Ph.D. Thesis, Technische Universiteit Delft, Delft, The Netherlands, 2015.
12. Robbins, B.A.; van Beek, V.M. Backward erosion piping: A historical review and discussion of influential factors. In Proceedings of the ASDO Dam Safety Conference, New Orleans, LA, USA, 13–17 September 2015; pp. 1–20.
13. Luo, G.; Rice, J.D.; Peng, S.; Cao, H.; Pan, H.; Xu, G. Modelling Initiation Stage of Backward Erosion Piping through Analytical Models. *Land* **2022**, *11*, 1970. [CrossRef]
14. Pan, H.; Rice, J.D.; Peng, S.; Cao, H.; Luo, G. Analytical Modeling with Laboratory Data and Observations of the Mechanisms of Backward Erosion Piping Development. *Water* **2022**, *14*, 3420. [CrossRef]
15. DeHaan, H.; Stamper, J.; Walters, B. *Mississippi River and Tributaries System 2011 Post-Flood Report*; USACE, Mississippi Valley Division: Vicksburg, MS, USA, 2012.
16. Glynn, E.; Quinn, M.; Kuszmaul, J. Predicting piping potential along Middle Mississippi River Levees. In Proceedings of the 6th International Conference on Scour and Erosion, Paris, France, 27–31 August 2012; pp. 1473–1480.
17. Semmens, S.N.; Zhou, W. Evaluation of environmental predictors for sand boil formation: Rhine–Meuse Delta, Netherlands. *Environ. Earth Sci.* **2019**, *78*, 1–11. [CrossRef]
18. Wolff, T.F. *Performance of Levee Underseepage Controls: A Critical Review*; Rep. No. ERDC/GSL TR-02-19; USACE: Washington, DC, USA, 2002.
19. Garcia Martinez, M.F.; Tonni, L.; Marchi, M.; Tozzi, S.; Gottardi, G. Numerical Tool for Prediction of Sand Boil Reactivations near River Embankments. *J. Geotech. Geoenviron. Eng.* **2020**, *146*, 06020023. [CrossRef]
20. Gutierrez, F. Sinkhole Hazards. In *Oxford Research Encyclopedia of Natural Hazard Science*; Oxford University Press: Oxford, UK, 2016; pp. 1–92.
21. Nguyen, T.K.; Benahmed, N.; Hicher, P.Y.; Nicolas, M. The Influence of Fines Content on the Onset of Instability and Critical State Line of Silty Sand. In *Bifurcation and Degradation of Geomaterials in the New Millennium, IWBDG 2014*; Chau, K.T., Zhao, J., Eds.; Springer Series in Geomechanics and Geoengineering; Springer: Berlin/Heidelberg, Germany, 2015.
22. Valois, R.; Camerlynck, C.; Dhemaied, A.; Guerin, R.; Hovhannissian, G.; Plagnes, V.; Rejiba, F.; Robain, H. Assessment of doline geometry using geophysics on the Quercy plateau karst (South France). *Earth Surf. Process. Landf.* **2011**, *36*, 1183–1192. [CrossRef]
23. Philippe, P.; Beguin, R.; Faure, Y.H. Contact erosion. In *Erosion in Geomechanics Applied to Dams and Levees*; John Wiley & Sons: Hoboken, NJ, USA, 2013; pp. 101–192.
24. Bianchi, E.; Borgatti, L.; Vittuari, L. The Medium- to Long-Term Effects of Soil Liquefaction in the Po Plain (Italy). In *Engineering Geology for Society and Territory*; Lollino, G., Ed.; Springer International Publishing: Cham, Switzerland, 2015; Volume 6, pp. 421–425.
25. Morton, L.W.; Olson, K.R. Sinkholes and sand boils during 2011 record flooding in Cairo (Illinois). *J. Soil Water Conserv.* **2015**, *70*, 49A–54A. [CrossRef]

26. Garner, S.J.; Fannin, R.J. Understanding internal erosion: A decade of research following a sinkhole event. *Hydropower Dams Int.* **2010**, *17*, 93–98.
27. Yin, Z.-Y.; Yang, J.; Laouafa, F.; Hicher, P.-Y. A framework for coupled hydro-mechanical continuous modelling of gap-graded granular soils subjected to suffusion. *Eur. J. Environ. Civ. Eng.* **2023**, *27*, 2678–2699. [CrossRef]
28. Dezert, T.; Fargier, Y.; Palma Lopes, S.; Cote, P. Geophysical and Geotechnical methods for fluvial levee investigation: A review. In *Engineering Geology*; Elsevier: Amsterdam, The Netherlands, 2019; 18p.
29. Karim, M.Z.; Tucker-Kulesza, S.E.; Rutherford, C.J.; Bernhardt-Barry, M. Geophysical Engineering to Identify Seepage Channels in the Hager Slough Levee. In *Eighth International Conference on Case Histories in Geotechnical Engineering*; Geotechnical Special Publications GSP 311; American Society of Civil Engineers: Reston, VA, USA, 2019.
30. Tourment, R.; Benahmed, N.; Nicaise, S.; Meriaux, P.; Salmi, A.; Rougé, M. Lessons learned on the damaged on the levees of the Agly River, analysis of the sand-boils phenomena, Q. 103 R.21. In Proceedings of the 26th ICOLD Congress, Vienna, Austria, 1–7 July 2018.
31. Puig, C.; Carozza, J.-M. Les changements de tracés des cours d'eau d'après les sources historiques et géomorphologiques dans la plaine du Roussillon depuis le XIIe siècle: Approche théorique et premiers résultats. In *Les Plaines Littorales en Méditerranée Nord-Occidentale, Regards Croisés D'histoire, D'archéologie et de Géographie, de la Protohistoire au Moyen Age*; Ropiot, V., Puig, C., Mazière, F., Eds.; Monique Mergoil: Paris, France; pp. 297–312.
32. Blanchy, G.; Saneiyan, S.; Boyd, J.; McLachlan, P.; Binley, A. ResIPy, an intuitive open source software for complex geoelectrical inversion/modeling. *Comput. Geosci.* **2020**, *137*, 104423. [CrossRef]
33. Côté, S. Internal Stability Criteria for Low-Plasticity Materials Subjected to Water Flow. Master's Thesis, University of Laval, Québec, QC, Canada, 2010; 237p. (In French).
34. Valois, R.; Galibert, P.Y.; Guerin, R.; Plagnes, V. Application of combined time-lapse seismic refraction and electrical resistivity tomography to the analysis of infiltration and dissolution processes in the epikarst of the Causse du Larzac (France). *Near Surf. Geophys.* **2016**, *14*, 13–22. [CrossRef]
35. Chavez Olalla, J.; Winkels, T.G.; Ngan-Tillard, D.J.M.; Heimovaara, T.J. Geophysical tomography as a tool to estimate the geometry of soil layers: Relevance for the reliability assessment of dikes. *Georisk Assess. Manag. Risk Eng. Syst. Geohazards* **2022**, *16*, 678–698. [CrossRef]